






**Long-range magnetic ordering in  $\text{Li}_2\text{MnGeO}_4$  and precursor short-range spin correlations**A. N. Korshunov <sup>1,\*</sup>, A. I. Kurbakov <sup>1,†</sup>, I. A. Safulina <sup>2,3</sup>, A. E. Susloparova <sup>1</sup>, V. Yu. Pomjakushin,<sup>4</sup> and Th. Mueller <sup>5</sup><sup>1</sup>*Petersburg Nuclear Physics Institute named by B.P. Konstantinov of NRC “Kurchatov Institute,” 188300 Gatchina, Russia*<sup>2</sup>*Laboratory for Quantum Magnetism, École Polytechnique Fédérale de Lausanne, CH-1015 Lausanne, Switzerland*<sup>3</sup>*Institut Laue-Langevin, 38042 Grenoble, France*<sup>4</sup>*Laboratory for Neutron Scattering and Imaging, Paul Scherrer Institute, CH-5232 Villigen, Switzerland*<sup>5</sup>*Jülich Centre for Neutron Science (JCNS) at Heinz Maier-Leibnitz Zentrum (MLZ), Forschungszentrum Jülich, Lichtenbergstrasse 1, D-85747 Garching, Germany*

(Received 26 June 2020; revised 30 November 2020; accepted 1 December 2020; published 15 December 2020)

Long-range magnetic ordering and short-range spin correlations in layered noncentrosymmetric orthogermanate  $\text{Li}_2\text{MnGeO}_4$  were studied by means of polarized and unpolarized neutron scattering. The combined Rietveld refinement of synchrotron and neutron powder diffraction data at room temperature within the  $Pmn2_1$  space group allowed us to specify the details of the crystal structure. According to the additional Bragg peaks in low-temperature neutron diffraction patterns a long-range antiferromagnetic ordering with the propagation vector  $k = (1/2\ 1/2\ 1/2)$  has been found below  $T_N \approx 8$  K. Symmetry analysis revealed the model of the ground state spin structure within the  $C_{ac}$  (no. 9.41) magnetic space group. It is represented by the noncollinear ordering of manganese atoms with a refined magnetic moment of  $4.9\ \mu_B/\text{Mn}^{2+}$  at 1.7 K, which corresponds to the saturated value for the high-spin configuration  $S = 5/2$ . Diffuse magnetic scattering was detected on the neutron diffraction patterns at temperatures just above  $T_N$ . Its temperature evolution was investigated in detail by polarized neutron scattering with the following XYZ-polarization analysis. Reverse Monte Carlo simulation of diffuse scattering data showed the development of short-range ordering in  $\text{Li}_2\text{MnGeO}_4$ , which is symmetry consistent on a small scale with the long-range magnetic state below  $T_N$ . The reconstructed radial spin-pair correlation function  $S(0)S(r)$  displayed the predominant role of antiferromagnetic correlations. It was found that spin correlations are significant only for the nearest magnetic neighbors and almost disappear at  $r \approx 12\ \text{Å}$  at 10 K. Temperature dependence of the diffuse scattering implies short-range ordering long before the magnetic phase transition. Besides, the spin arrangement was found to be similar in both cases above and below  $T_N$ . As a result, an exhaustive picture of the gradual formation of magnetic ordering in  $\text{Li}_2\text{MnGeO}_4$  is presented.

DOI: [10.1103/PhysRevB.102.214420](https://doi.org/10.1103/PhysRevB.102.214420)**I. INTRODUCTION**

The long-range spin ordering in magnetic materials is a result of competing spin exchange interactions between magnetic atoms, which usually involve nonmagnetic ligand orbitals. The crystal structure determines the variety of magnetic phenomena. The prediction of the ground magnetic state is not an easy task even for a detailed studied crystal lattice, and it requires the application of numerical methods such as density functional theory (DFT) calculations. The situation is more complicated with the presence of frustration and magnetic anisotropy in real systems.

According to Landau theory [1], a magnetic phase transition to the ordering state is the result of spontaneous symmetry breaking. The critical behavior near the phase transition point is uniquely determined by the universality class of the magnetic system. Magnetic correlations become increasingly important when spins tend to form a certain ordering configuration, thereby minimizing the free energy [2–5]. The

study of the spin correlations is important to understand the microscopic mechanisms of the magnetic ordering.

The present work is devoted to a comprehensive study of the phase transition from the paramagnetic to the ordered magnetic state in orthorhombic complex oxide  $\text{Li}_2\text{MnGeO}_4$ . It belongs to the large  $A_2MXO_4$  structural family, which exhibits rich polymorphism with various crystal structures that could be stabilized depending on the synthesis conditions (see Ref. [6] and references therein). In these compounds, the tetrahedral ordering of all cations is formed by hexagonal close-packing of the oxygen atoms. Despite nominally the same identical chemical composition, different types of the cationic orderings and distortions can lead to various crystal structures. For example, the monoclinic  $P2_1/n$  and the orthorhombic  $Pmn2_1$  or  $Pmnb$  space groups were reported for both  $\text{Li}_2\text{MnSiO}_4$  and  $\text{Li}_2\text{FeSiO}_4$  compounds [7–10]. This rich polymorphism associated with low transition energies has attracted attention due to the use of alkali-metal contained  $A_2MXO_4$  compounds as cathode materials. Their electrical and chemical properties have been extensively studied in recent years ([6] and references therein, [9–12]). The most actively investigated compounds in this series are based on magnetic cations  $M^{2+} = \text{Co}, \text{Fe}, \text{and Mn}$ , nevertheless

\*Corresponding author: [artem.korshunov91@gmail.com](mailto:artem.korshunov91@gmail.com)†Corresponding author: [kurbakov\\_ai@npni.nrcki.ru](mailto:kurbakov_ai@npni.nrcki.ru)

magnetic properties of the  $A_2MXO_4$  system remain relatively unexplored.

Recently, a long-range antiferromagnetic (AFM) ordering was reported only experimentally by means of neutron powder diffraction for  $\beta_1$ - $\text{Li}_2\text{CoSiO}_4$  and  $\gamma_0$ - $\text{Li}_2\text{MnSiO}_4$  [13]. Besides, bulk magnetic properties and DFT calculations of spin exchange constants were published for  $\text{Li}_2\text{MnSiO}_4$ ,  $\text{Na}_2\text{MnSiO}_4$ ,  $\text{Li}_2\text{MnGeO}_4$ , and  $\text{Na}_2\text{MnGeO}_4$  [14]. In particular, it was found that  $\text{Li}_2\text{MnGeO}_4$  undergoes a three-dimensional antiferromagnetic ordering at the Néel temperature  $T_N = 8.1 \pm 0.5$  K with Weiss temperature  $\Theta = -27$  K. The negative  $\Theta$  value indicates predominantly mainly AFM interactions in the compound. The magnetic interaction scheme includes five AFM exchanges with the largest one along the  $c$  axis. A stable collinear spin arrangement with a weak frustration was found that can be attributed to the presence of spin-frustrated exchange triangles in the crystal structure. However, the actual magnetic ground state of  $\text{Li}_2\text{MnGeO}_4$  remains unknown and awaits experimental investigation.

The choice of  $\text{Li}_2\text{MnGeO}_4$  for further research is caused by several reasons. First of all, the compound is layered, not 3D, like most of the  $A_2MXO_4$  family. In particular, high ionic conductivity is caused by the presence of the allocated alkali-metal ion layers. The ordering of oxygen tetrahedra with  $M/X$  ions in the center leads to the spin-frustrated triangles of manganese ions [14]. With antiferromagnetic interactions, there is a spin coupling conflict between the nearest neighbors, and such a system becomes magnetically frustrated. Finally, while in many related compounds, for example, in  $\text{Li}_2\text{MnSiO}_4$ , half of the tetrahedra have the opposite orientation which leads the system to be centrosymmetric, all the tetrahedra in  $\text{Li}_2\text{MnGeO}_4$  are directed in the same way, perpendicular to the oxygen close-packed layers, and the structure is non-centrosymmetric, i.e., it suggests the existence of interesting nonlinear physical properties.

Hereafter, we report on properties of  $\text{Li}_2\text{MnGeO}_4$ , probed by neutron scattering measurements with polarized and unpolarized techniques. With the combined Rietveld analysis of synchrotron and neutron powder diffraction data, the details of the crystal structure and its individual fragments are refined. The main attention is paid to the study of the magnetic ordering in the system. The temperature evolution of the magnetic neutron scattering has shown the transition from the short-range to the long-range magnetic ordering. We propose the model of the magnetic ground state at the lowest obtained temperature of 1.7 K, which is experimentally determined based on the magnetic symmetry analysis and profile refinement of neutron diffraction data. The temperature evolution of the spin-pair correlation function is received using Monte Carlo calculations for the diffuse magnetic neutron scattering observed above  $T_N$ . Analysis of the magnetic correlations reveals the information about the short-range magnetic ordering. This study provides comprehensive information on the magnetic ordering in  $\text{Li}_2\text{MnGeO}_4$ .

## II. EXPERIMENT

Polycrystalline  $\text{Li}_2\text{MnGeO}_4$  was prepared by conventional solid-state synthesis, as previously reported [14]. For the

present neutron and synchrotron diffraction study, a larger batch was prepared from the same reagents by the same route.

Structural investigations at room temperature (RT) were carried out using the SpLine BM25 beamline at the European Synchrotron Radiation Facility (Grenoble, France) using monochromatic x-ray radiation with a wavelength of 0.621 Å. The powder sample was sealed into a thin-walled borosilicate capillary with 0.5-mm inner diameter. Data were collected using a pointlike detector in the  $2\theta$  range from  $6^\circ$  to  $43^\circ$  with  $0.01^\circ$  steps. A standard  $\text{LaB}_6$  sample was measured before the experiment to obtain the instrumental resolution function of the BM25 diffractometer.

Neutron diffraction studies were performed at the spallation neutron source SINQ in the Paul Scherrer Institute (Villigen, Switzerland). For the crystal structure refinement, data from high-resolution powder diffractometer HRPT were obtained with two neutron wavelengths  $\lambda = 1.494$  and  $1.886$  Å. The sample was placed in a standard vanadium cylindrical container with an inner diameter of 6 mm. Measurements were carried out at RT and at the lowest reachable temperature  $T = 1.9$  K in the angular range  $4$ – $164^\circ$  with  $0.05^\circ$  steps. The Rietveld refinement of neutron and synchrotron data at RT was performed in the combined mode in order to get the precise information about ordering of both heavy and light atoms in the crystal structure. The low-temperature neutron diffraction measurements were conducted at the cold neutron powder diffractometer DMC with the incident wavelength  $\lambda = 2.458$  Å. This instrument is efficient for the analysis of the magnetic phase transitions and for the determination of magnetic structures. The sample was in the same vanadium container as at the HRPT. The standard orange cryostat was used for measurements at several temperatures between 1.7 and 30 K near the magnetic phase transition. Neutron diffraction patterns were collected in the  $2\theta$  range of  $5$ – $86^\circ$  with  $0.1^\circ$  steps. All the diffraction data were analyzed by means of the Rietveld method using the FULLPROF suite [15].

A polarized neutron scattering experiment was carried out on the diffuse scattering neutron time-of-flight spectrometer DNS [16] at the MLZ (Garching, Germany). The incident wavelength was  $\lambda = 4.74$  Å that allows us to collect data in the elastic  $Q$  range from 0.1 to  $2.3$  Å $^{-1}$ . The main assignment of the instrument is to distinguish different contributions to the total neutron scattering cross section such as nuclear coherent, nuclear incoherent, and magnetic scattering through XYZ-polarization analysis [17]. In order to receive temperature evolution of the magnetic correlations in  $\text{Li}_2\text{MnGeO}_4$ , measurements were conducted at temperatures of 3.5, 10, 20, 30, 50, 70, 100, and 300 K. DNS data analysis was performed using the reverse Monte Carlo (RMC) method [18], which is implemented in the SPINVERT program [19].

## III. RESULTS

### A. Crystal structure

The results of the combined profile analysis of the synchrotron and neutron powder diffraction at room temperature are shown in Fig. 1. The data were successfully analyzed using the initial structure model previously determined using

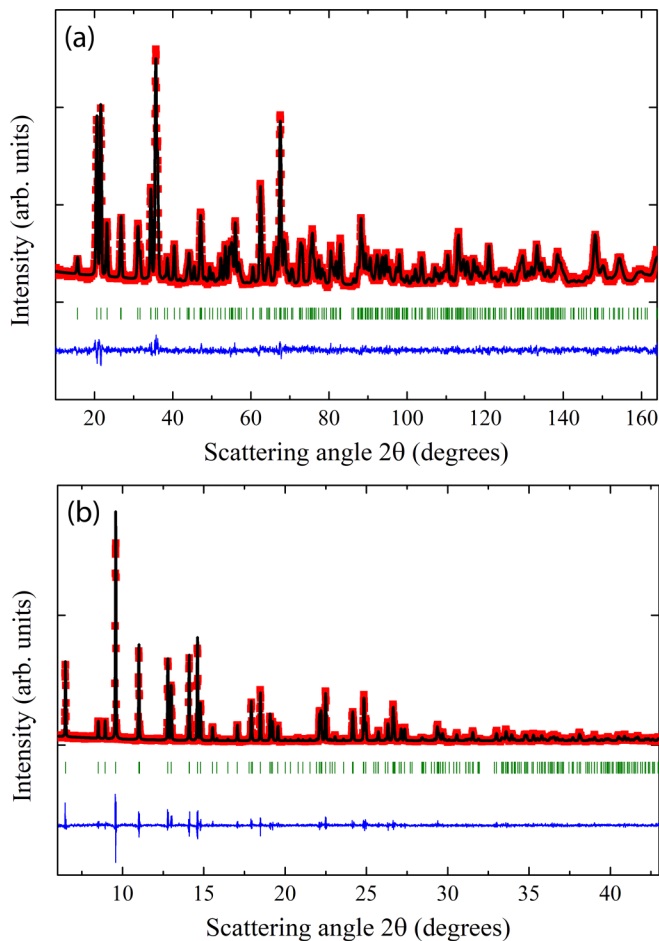


FIG. 1. The combined Rietveld refinement of RT (a) neutron (HRPT,  $\lambda = 1.494 \text{ \AA}$ ) and (b) synchrotron (BM25,  $\lambda = 0.621 \text{ \AA}$ ) diffraction data for  $\text{Li}_2\text{MnGeO}_4$ . The red dots represent the experimental data, the black lines show the calculated intensity, the blue lines indicate the difference between experimental and simulated diffraction patterns, and the green ticks show the angular positions of the Bragg reflections.

laboratory x-ray diffraction [14]. The refined atomic coordinates with thermal parameters in view of the  $Pmn2_1$  space group are indicated in Table I. Since all the atoms are located at Wyckoff positions with freely variable coordinates along the  $c$  axis, the  $z$  coordinate of the Mn was manually fixed to zero. A small, but noticeable degree of Li/Mn mixing at 2.5(4) wt% was found. Taking this into account,  $\chi^2$  slightly improves from 3.15 to 3.08, therefore we admit that the observed mixing may be due to the incomplete occupation of the atomic positions. The refined lattice parameters are completely consistent with the results obtained with those obtained in Ref. [14] (Table II). The small difference between neutron and synchrotron data refinement is associated with the different interaction mechanisms of radiation with matter and it can also be explained by the fact that the sample temperature was not exactly equal in these two experiments.

The crystal structure of  $\text{Li}_2\text{MnGeO}_4$  is based on hexagonal close-packing of oxygen atoms, where all cations are in a distorted tetrahedral environment (Fig. 2). In comparison to  $\text{Li}_2\text{MnSiO}_4$  [13], here all tetrahedra are pointed in the same

TABLE I. Crystallographic data of  $\text{Li}_2\text{MnGeO}_4$  within the framework of the  $Pmn2_1$  (no. 31) space group at room temperature observed using combined neutron (HRPT,  $\lambda = 1.494 \text{ \AA}$ ) and synchrotron (BM25,  $\lambda = 0.621 \text{ \AA}$ ) powder diffraction data refinement. To eliminate the uncertainty related with float origin, the  $z$  coordinate of the Mn atom was fixed to zero. Global  $\chi^2 = 3.08$ . Agreement factors are indicated in Table II.

Atom	Site	$x/a$	$y/b$	$z/c$	$B_{\text{iso}}(\text{\AA}^2)$
Li	4b	0.2493(17)	0.3296(23)	0.0077(43)	1.07(17)
Mn	2a	1/2	0.8260(8)	0 (fixed)	0.63(9)
Ge	2a	0	0.8226(5)	0.0146(19)	0.61(4)
O1	4b	0.2222(5)	0.6733(7)	0.8985(17)	0.59(6)
O2	2a	0	0.1306(9)	0.9128(19)	0.72(8)
O3	2a	1/2	0.1821(10)	0.8616(17)	0.64(9)

direction and border only through the vertices. The cations are displaced from the center of tetrahedra, but the average distance between the atoms agrees well with the sums of the ionic radii according to Shannon [21].

The magnetic lattice in  $\text{Li}_2\text{MnGeO}_4$  is formed by  $\text{Mn}^{2+}$  ions, where each Mn has 12 magnetic neighbors in the distorted cuboctahedron (Fig. 3). Due to the close-packed structure, magnetic interactions between neighboring ions are mainly determined by super-super exchanges, which engage various possible pathways involving Li, O, and Ge ions. The neutron powder diffraction on HRPT and DMC instruments did not show any crystal structure phase transition down to 1.7 K. The lattice parameters are naturally decreasing upon cooling, while all the atoms remain in their crystallographic positions [20].

## B. Long-range magnetic ordering

Temperature dependence of neutron powder diffraction patterns at the DMC instrument show the appearance of the additional Bragg peaks due to the long-range magnetic ordering [Fig. 4(a)], which is consistent with magnetic susceptibility data for  $\text{Li}_2\text{MnGeO}_4$  [14]. A small impurity magnetic peak near  $2\theta \approx 28^\circ$  was found. Its magnetic nature was later confirmed by polarized neutron measurements. Most likely, the undescribed peak is associated with MnO impurity according to the temperature range of the peak existence and its angular position corresponding to the first intense reflection of antiferromagnetically ordered MnO [22]. However, the refined concentration is less than 1%, and no additional reflections from the crystal phase were detected even in synchrotron and neutron powder diffraction data at room temperature. Therefore, this does not prevent us from analyzing the magnetic Bragg scattering of the main phase.

Clear diffuse scattering near the first magnetic reflection can be seen above  $T_N$ . This feature is associated with the presence of spin correlations due to the short-range magnetic ordering, which we will discuss in the next section. The additional magnetic peaks correspond to the commensurate long-range spin ordering with the propagation vector  $k = (1/2 \ 1/2 \ 1/2)$ , which is constant at the temperatures 1.7–7 K. That is, the magnetic unit cell is doubled in all directions in

TABLE II. Crystal lattice parameters obtained by the profile refinement of neutron (HRPT,  $\lambda = 1.494 \text{ \AA}$ ) and synchrotron (BM25,  $\lambda = 0.621 \text{ \AA}$ ) diffraction patterns at 300 K in comparison with the results obtained with the laboratory x-ray diffractometer in Ref. [14]. The last column corresponds to low-temperature neutron diffraction data (HRPT,  $\lambda = 1.886 \text{ \AA}$ ) at  $T = 1.9 \text{ K}$  [20].

	Lab x-ray (RT) [14]	Neutrons (RT)	Synchrotron (RT)	Neutrons (1.9 K)
$a$ ( $\text{\AA}$ )	6.46751(7)	6.46847(16)	6.47615(7)	6.46728(2)
$b$ ( $\text{\AA}$ )	5.47639(5)	5.47905(14)	5.48519(6)	5.46699(2)
$c$ ( $\text{\AA}$ )	5.05380(5)	5.05394(11)	5.05978(5)	5.04710(2)
$V$ ( $\text{\AA}^3$ )	179.00	179.117(7)	179.738(3)	178.448(1)
$R_p$		4.70%	9.42%	2.76%
$R_{wp}$		5.99%	11.9%	3.59%
$R_{\text{exp}}$		4.70%	5.72%	2.23%
$\chi^2$		1.62	4.35	2.60

comparison to the crystallographic ones due to the translational periodicity of the magnetic structure.

The symmetry analysis performed with the program MAXMAGN [23] from the Bilbao Crystallographic Server for the  $Pmn2_1$  space group and the propagation vector  $k$  reveal two maximal magnetic subgroups  $C_{ac}$  (no. 9.41) and  $C_{am}$  (no. 8.36) (in Belov-Neronova-Smirnova setting [24]). Both of them are noncentrosymmetric and allow a nonzero magnetic moment at the Mn sites. The corresponding spin structure models were tried out to describe the experimental neutron diffraction data. The main results of the refinement are shown in Table III. Both magnetic space groups have similar magnetic symmetry according to the transformation of the magnetic moments between the different magnetic sites inside the unit cell. However, the crystallographic position of the Mn atom in the  $C_{am}$  group splits into two sites with different directions of the magnetic moments (Table III). The model of the magnetic structure for each magnetic space group was refined according to neutron powder diffraction data at 1.7 K, allowing all magnetic moment projections (3 coefficients for one atom within  $C_{ac}$  and  $2 + 1$  for two atoms within  $C_{am}$  magnetic space group) to refine independently. It was found that a slightly better agree-

ment between experimental and calculated powder diffraction patterns was for the  $C_{ac}$  magnetic group [Fig. 4(b)], with a refined magnetic moment shown in Table III. The corresponding spin structures are presented in Fig. 5. It is worth emphasizing that these magnetic space groups allow us to use the magnetic unit cell, which is only four times bigger than the crystallographic one, instead of the unit cell associated with the propagation vector, which is eight times bigger [(Fig. 4(d)]. With the  $C_{am}$  space group, the values of the magnetic moments at the neighboring sites inside the unit cell differ, as well as their directions, and we consider this situation extremely unlikely. Thereby, the observed noncollinear spin arrangement with the  $C_{ac}$  magnetic space group is symmetrically equivalent to the model that was expected from previous density functional theory calculations [14] (Fig. 5). The magnetic moments' inclination can be caused by the presence of various superexchange pathways through the nonmagnetic atoms,

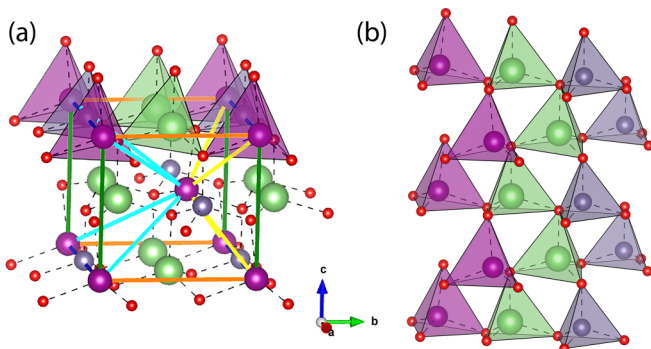


FIG. 2. (a) Refined crystal structure of  $\text{Li}_2\text{MnGeO}_4$  with the tetrahedral environment of oxygens (red balls). Magenta, light green, and grey balls show the Mn, Li, and Ge sites respectively in the  $Pmn2_1$  space group. All tetrahedra border each other only through the vertices. Couplings between magnetic  $\text{Mn}^{2+}$  ions indicate the main spin exchange paths with colors used in Ref. [14]. (b) Fragment of  $\text{Li}_2\text{MnGeO}_4$  crystal structure in the  $bc$  crystallographic plane. Some tetrahedra are excluded for clarity.

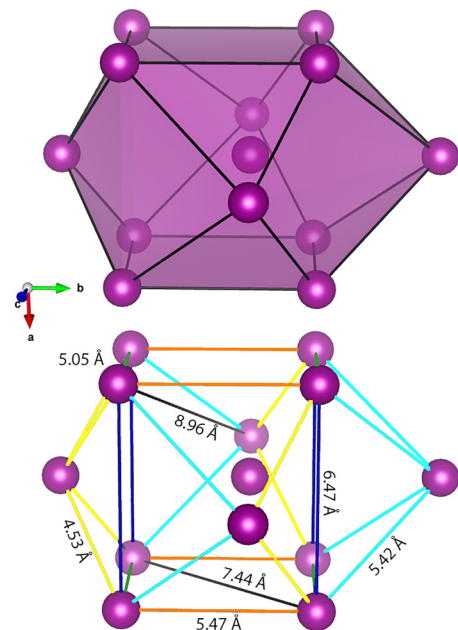


FIG. 3. General view of the distorted cuboctahedron formed by 12 nearest Mn neighbors. The main distances between magnetic atoms at  $T = 1.9 \text{ K}$  are indicated in the bottom image. Couplings between magnetic  $\text{Mn}^{2+}$  ions indicate the main spin exchange paths with colors used in Ref. [14].

TABLE III. Comparison of the profile refinement using two different models for  $\text{Li}_2\text{MnGeO}_4$  spin structure.

	$C_{ac}$ (no. 9.41)	$C_{am}$ (no. 8.36)	
Atom	Mn 0 0.08725 0.25	Mn1 0 0.08725 0.25	Mn2 0.25 0.91275 0.50
Magnetic moment	(Mx, My, Mz)	(Mx,0,0)	(0, My, Mz)
	1.75(3), 2.45(4), 3.86(2)	2.46(5), 0, 0	0, 3.47(5), 5.46(3)
$M_{\text{tot}}(\mu_B)$	4.9	2.46	6.47
$R_p$	3.84%		3.84%
$R_{\text{exp}}$	2.28%		2.28%
Magnetic $R$ factor	6.02%		6.35%
$\chi^2$	4.59		4.59

which, in addition, can lead to the orbital ordering in the system.

The total value of the magnetic moment at 1.7 K is  $4.9 \mu_B/\text{Mn}$ , which is almost equal to the expected value

$M_s = gS\mu_B \approx 5 \mu_B/\text{Mn}$  for high-spin  $S = 5/2d^5 \text{Mn}^{2+}$ . On the other hand, the observation of the increased moment of  $6.47 \mu_B$  in the frame of the  $C_{am}$  magnetic space group does not seem appropriate, which emphasizes the choice of non-collinear ordering using the  $C_{ac}$  solution for  $\text{Li}_2\text{MnGeO}_4$ .

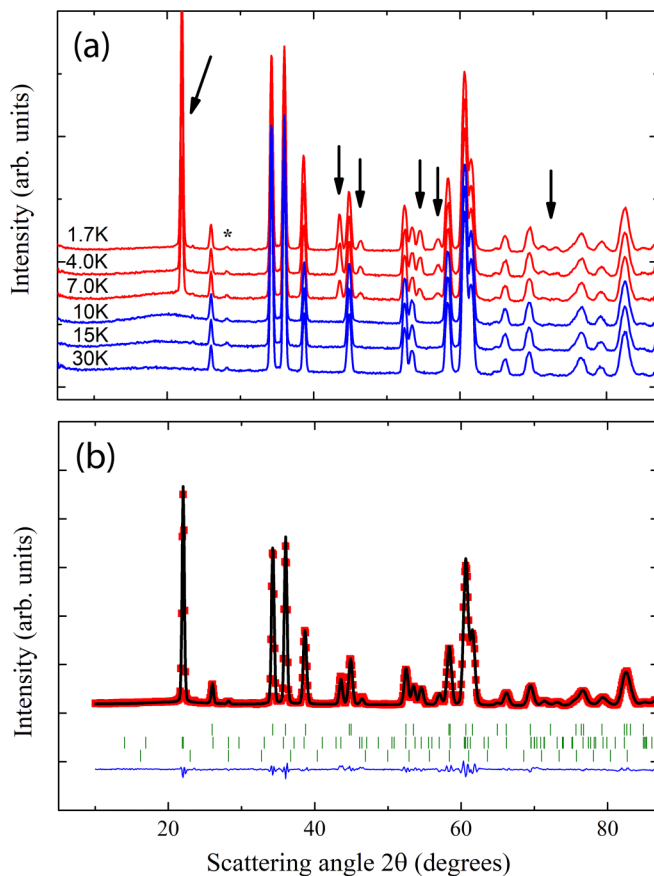


FIG. 4. (a) Low temperature neutron diffraction patterns of  $\text{Li}_2\text{MnGeO}_4$  (DMC,  $\lambda = 2.46 \text{ \AA}$ ). Arrows are pointing to the most intense additional reflections associated with the magnetic scattering appearing at the temperatures  $T \leq 7 \text{ K}$ . Asterisk marks the position of the magnetic peak from possible MnO impurity. (b) Experimentally observed (red dots) and calculated (black solid line) neutron diffraction pattern at 1.7 K. The difference between the experimental and calculated patterns is shown by the solid blue line. The two upper sets of vertical green bars indicate the positions of the nuclear and magnetic Bragg peaks from  $\text{Li}_2\text{MnGeO}_4$ , respectively. The bottom ticks indicate the position of the combined nuclear and magnetic Bragg peaks from possible MnO impurity.

### C. Diffuse scattering and short-range magnetic ordering

As mentioned in the previous section, the broad diffuse scattering near the first magnetic reflection was detected in the neutron powder diffraction experiments above  $T_N$  [Fig. 4(a)]. To more thoroughly study its temperature evolution, we performed polarized neutron diffraction at the DNS instrument. The following XYZ-polarization analysis [17] based on the Maleev-Blume theory [25] was performed to separate magnetic, nuclear incoherent, and nuclear spin coherent contributions to the total neutron scattering cross section. The temperature dependence of the magnetic neutron scattering signal in the 10–300-K range is presented in Fig. 6. The data show the broad peak associated with the spin

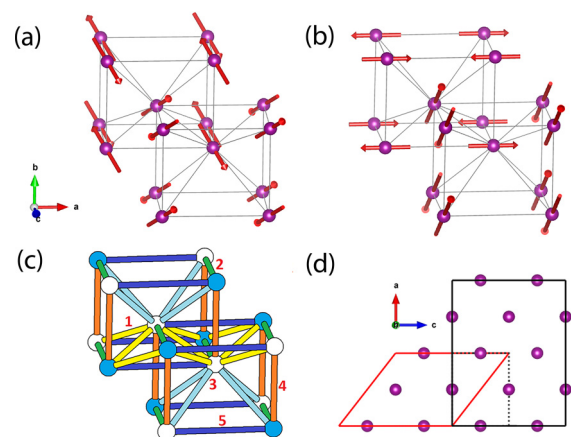


FIG. 5. Spin structure models of  $\text{Li}_2\text{MnGeO}_4$  at 1.7 K. (a) noncollinear ordering using the  $C_{ac}$  magnetic space group. (b) Two-sublattice model with two split Mn positions in the  $C_{am}$  magnetic space group. (c) Spin exchange paths of the collinear spin arrangement expected from DFT calculations (figure is adopted from Ref. [14]); shaded and unshaded spheres represent up-spin and down-spin  $\text{Mn}^{2+}$  sites, respectively. (d) Comparison of different unit cells. Dashed black, black, and red lines denote (i) crystal unit cell with lattice parameters  $(a, b, c)$ , (ii) unit cell  $(2a, 2b, 2c)$  associated with propagation vector  $k$ , and (iii) magnetic unit cell in standard settings  $(-2c, 2b, a+c)$ , respectively.

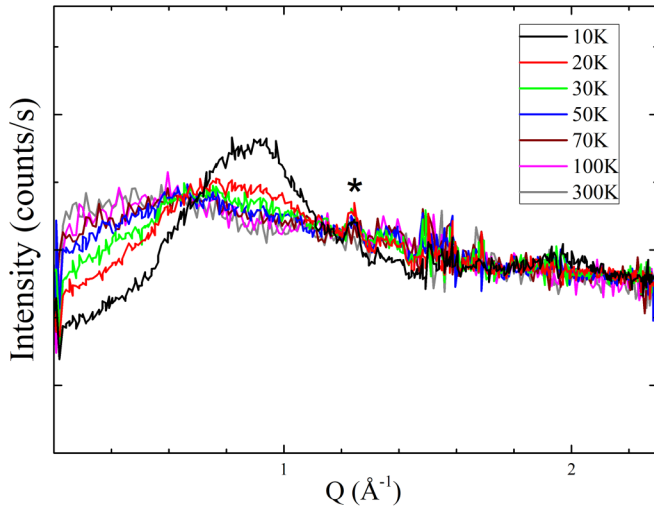


FIG. 6. Set of the magnetic neutron scattering cross-sections for  $\text{Li}_2\text{MnGeO}_4$  after  $XYZ$ -polarization analysis (DNS,  $\lambda = 4.74 \text{ \AA}$ ). Asterisk marks the position of the magnetic peak from possible MnO impurity.

correlations without any static long-range magnetic order. The peak becomes monotonically narrower with temperature decreasing. This experimental result indicates that the spins in the lattice correlate with each other long before the magnetic phase transition. At high temperature, the observed pattern completely corresponds to the neutron scattering from paramagnets, which means the absence of any magnetic ordering in the system.

Such broad features associated with spin correlations cannot be fitted using the conventional Rietveld refinement, but can be described by the modeling using the reverse Monte Carlo method. This approach is entirely independent of the spin Hamiltonian and does not provide a unique solution for spin structure. The RMC analysis allows a reconstruction of a radial spin-pair correlation function by fitting diffuse scattering from powder with simulated scattering from a specified large spin configuration. In the present work, we have used the SPINVERT program [19], which was successfully applied recently to a number of disordered magnetic systems [26–28]. For calculations we used a  $20 \times 20 \times 20$  box with 16 000 randomly oriented spins, fixed to their crystallographic positions.

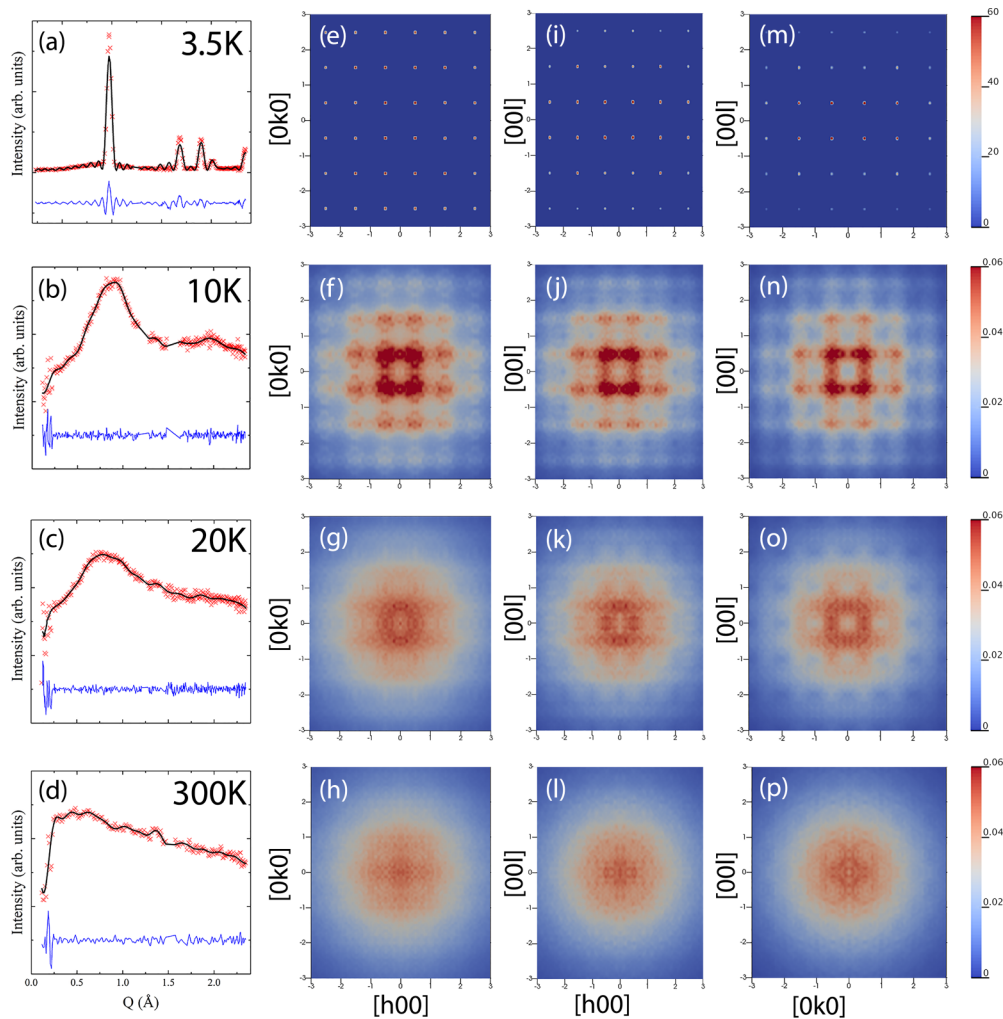


FIG. 7. (a)–(d) Results of the RMC analysis of diffuse magnetic scattering data for  $\text{Li}_2\text{MnGeO}_4$  at  $T = 3.5; 10; 20; 300 \text{ K}$ . Red crosses, black and blue solid lines indicate the observed and calculated patterns and their difference, respectively. (e)–(p) Reconstructed reciprocal space maps for  $(hk0.5)$ ,  $(h0.5l)$ , and  $(0.5kl)$  scattering planes.

Refinements were performed for 100 proposed moves per magnetic moment, which demonstrated satisfactory convergence. To minimize the statistical noise, the calculated neutron scattering was averaged over 20 independent spin configurations for each temperature.

The simulated curves for diffuse scattering with experimental data at different temperatures are presented in Figs. 7(b)–7(d). Two regions near  $Q \approx 1.2$  and  $1.5 \text{ \AA}^{-1}$  have been excluded from the final refinements: the first is related with the magnetic peak from possible MnO impurity, which is present in the data up to 70 K; and the second due to the up-down features in the area of the intense nuclear reflection. The resulting spin configurations were used to reproduce the reciprocal space maps using the SCATTY program [29]. The  $(hk0.5)$ ,  $(h0.5l)$ , and  $(0.5kl)$  scattering planes are shown in Figs. 7(e)–7(p). The magnetic intensity is concentrated around the points at which all three indices  $h$ ,  $k$ , and  $l$  are half-integer. It indicates that observed short-range ordering is in full agreement with the propagation vector  $k = (1/2 \ 1/2 \ 1/2)$  of the ordered magnetic state below  $T_N$ . Therefore, the short-range spin correlations inherit the translation symmetry of the ground magnetic state, but this ordering remains for a few neighbors only. On the other hand, a rodlike diffuse magnetic neutron scattering was found along all crystallographic directions  $[h00]$ ,  $[0k0]$ , and  $[00l]$ . This observation indicates a decrease in the correlations between the magnetic moments in the system during the phase transition from the long-range order to the paramagnetic state. With the temperature increasing all the sharp features disappear and only diffuse rods remain visible in the scattering planes at 20 K. Rodlike features indicate the origin of the Bragg reflection broadening when the short-range correlations became important. The nearly stable picture of the scattering patterns suggests that there are no significant changes in the magnetic system, except for a natural decrease in the correlation length. Finally, the remaining smeared scattering at high temperature corresponds to the pure paramagnetic response.

The reliability of the magnetic system modeling using the SPINVERT program could be emphasized by the 3.5-K data calculations (Fig. 7, upper row), where clear magnetic Bragg reflections are visible. We received single-crystal reciprocal space maps, which indicate long-range magnetic ordering with the propagation vector  $k = (1/2 \ 1/2 \ 1/2)$ . The observed result is in complete agreement with the Rietveld refinement of neutron powder diffraction data, although we have not received a microscopic model of spin ordering.

To understand the nature of the diffuse scattering in  $\text{Li}_2\text{MnGeO}_4$ , the spin-pair correlation function in real space  $S(0)S(r)$  was calculated [Fig. 8(a)]. The data were obtained by averaging 20 independent spin configurations, although numerical variations between different configurations were quite small. Each point in Fig. 8(a) corresponds to a certain distance between spins in accordance with the crystal structure. The magnetic moments are parallel to each other in the case of a positive value of the spin-pair correlation function and antiparallel in the opposite case. It was found that the system includes both AFM and FM couplings, but with a clear predominance of the first one. AFM couplings exist along the main crystallographic axes form the short-range ordered structure, which is consistent with the spin structure below  $T_N$  and

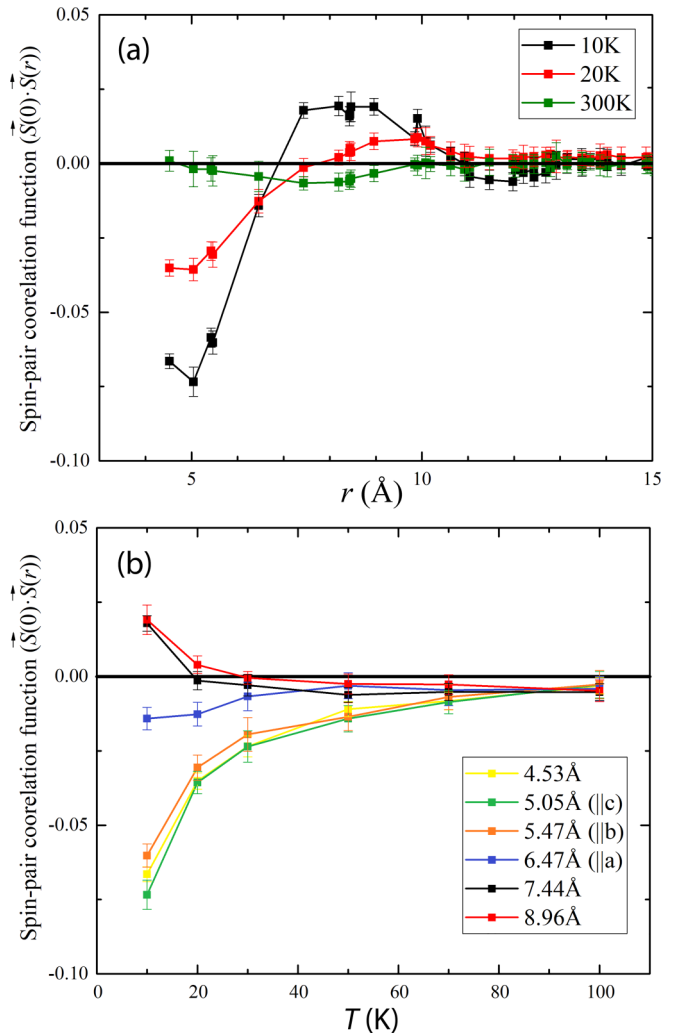


FIG. 8. (a) Spin-pair correlation function  $S(0)S(r)$  in direct space for several temperatures. Each point on the graph corresponds to the certain distance between the magnetic neighbors, similar to Fig. 3. (b) Temperature dependence of the magnetic correlations for the first shells with indicated distances.

the propagation vector  $k = (1/2 \ 1/2 \ 1/2)$ . It is represented by AFM rectangle lattices in the  $ab$ ,  $bc$ , and  $ac$  planes. The data also suggest that the correlations between magnetic moments on the diagonals of the rectangles are somewhat weaker and ferromagnetic. At the same time, the smallest AFM coupling along the  $a$  axis indicates a decrease of the spin correlation length in this direction. The corresponding distance between two  $\text{Mn}^{2+}$  along the  $a$  axis is relatively large, which implies involving more nonmagnetic neighbors to the magnetic interaction path. This has a direct impact on the spin correlations in the compound, which requires additional careful examination of super-super exchange interactions beyond the current work.

Note that the spin correlations function damped sharply with increasing distance and almost fade out at  $r \approx 12 \text{ \AA}$ . The corresponding correlation length is typical for the short-range ordering when only nearest neighbors interact. All the spin-pair correlations demonstrate the similar temperature behavior presented in Fig. 8(b), including the natural decrease in correlation values during the heating. At high temperatures,

correlations between magnetic neighbors are practically absent, which corresponds to the paramagnetic state.

Observed diffuse magnetic neutron scattering above  $T_N$  is associated with strong spin-spin correlations between the nearest  $Mn^{2+}$  neighbors. We have demonstrated that spins in the lattice begin to correlate with each other long before the magnetic phase transition. Such behavior has been observed for previously studied magnetic insulator compounds [30,31]. The RMC analysis showed that the symmetry of short-range ordering within several nearest neighbors is in accordance with the spin structure in the ordered state. This indicates the gradual formation of long-range magnetic ordering in  $Li_2MnGeO_4$ . The results of this work are important for a deeper understanding of the magnetic interaction scheme, which is responsible for the magnetic ordering formation in the studied and other structure-related compounds.

#### IV. CONCLUSIONS

In conclusion, we have studied the details of the crystal and magnetic ordering in  $Li_2MnGeO_4$  using the combination of synchrotron and neutron scattering techniques. The crystal structure within the  $Pmn2_1$  space group has been confirmed and refined at low and high temperatures. Powder diffraction analysis did not show any structural phase transition in a wide temperature range from 1.7 to 300 K. The compound undergoes a magnetic phase transition to the AFM long-range ordered state at  $T_N \approx 8$  K. The model of the spin structure within the  $C_{2c}$  magnetic space group was proposed based on the Rietveld refinement of the neutron powder diffraction data. The corresponding noncollinear magnetic ordering is

consistent with previous theoretical calculations, but in fact it suggests a more complex magnetic phase. The magnitude of the ordered magnetic moment derived from the neutron diffraction data at 1.7 K is  $4.9 \mu_B/Mn$ , which is almost equal to the expected value for  $Mn^{2+}$ . We have also probed the temperature evolution of the magnetic correlations in  $Li_2MnGeO_4$  using polarized neutron scattering. The reverse Monte Carlo analysis showed the short-range ordering above  $T_N$ , which is symmetrically identical on a small scale to the long-range magnetic structure. We have demonstrated that the spins in the lattice begin to correlate with each other long before the magnetic phase transition. The obtained correlation length of 12 Å is typical for the systems with the nearest neighboring interacted spins.

Thus, this work provides a comprehensive picture on the gradual formation of the magnetic ordering in  $Li_2MnGeO_4$ .

#### ACKNOWLEDGMENTS

The authors are thankful to Dr. V. Nalbandyan (SFedU, Russia) for the sample synthesis; Dr. L. Keller (LNS, PSI, Switzerland), M. D. Kuchugura (NRC “Kurchatov Institute,” PNPI, Russia), and Dr. A. A. Mistonov (SPbU, Russia) for their help with the diffraction experiments. The experiments were performed at the SpLine BM25 at ESRF (Grenoble, France); the HRPT and the DMC, Swiss neutron spallation source SINQ at PSI; and at DNS operated by JCNS at the Heinz Maier-Leibnitz Zentrum (MLZ), Garching, Germany. The reported study was funded by Russian Science Foundation according to the research Project No. 18-12-00375.

- 
- [1] L. D. Landau and E. M. Lifshitz, *Statistical Physics, Volume V of Course of Theoretical Physics* (Pergamon, Oxford, 1980).
- [2] K. Yamada, C. H. Lee, K. Kurahashi, J. Wada, S. Wakimoto, S. Ueki, H. Kimura, Y. Endoh, S. Hosoya, G. Shirane, R. J. Birgeneau, M. Greven, M. A. Kastner, and Y. J. Kim, Doping dependence of the spatially modulated dynamical spin correlations and the superconducting-transition temperature in  $La_{2-x}Sr_xCuO_4$ , *Phys. Rev. B* **57**, 6165 (1998).
- [3] C. Castelnovo, R. Moessner, and S. L. Sondhi, Magnetic monopoles in spin ice, *Nature (London)* **451**, 42 (2008).
- [4] S. A. Kivelson, I. P. Bindloss, E. Fradkin, V. Oganesyan, J. M. Tranquada, A. Kapitulnik, and C. Howald, How to detect fluctuating stripes in the high-temperature superconductors, *Rev. Mod. Phys.* **75**, 1201 (2003).
- [5] I. Morgenstern and K. Binder, Magnetic correlations in two-dimensional spin-glasses, *Phys. Rev. B* **22**, 288 (1980).
- [6] C. Masquelier and L. Croguennec, Polyanionic (phosphates, silicates, sulfates) frameworks as electrode materials for rechargeable Li (or Na) batteries, *Chem. Rev.* **113**, 6552 (2013).
- [7] M. Bini, S. Ferrari, C. Ferrara, M. C. Mozzati, D. Capsoni, A. J. Pell, G. Pintacuda, P. Canton, and P. Mustarelli, Polymorphism and magnetic properties of  $Li_2MSiO_4$  ( $M = Fe, Mn$ ) cathode materials, *Nat. Sci. Rep.* **3**, 3452 (2013).
- [8] A. Boulineau, C. Sirisopanorn, R. Dominko, A. R. Armstrong, P. G. Bruce, and C. Masquelier, Polymorphism and structural defects in  $Li_2FeSiO_4$ , *Dalton Trans.* **39**, 6310 (2010).
- [9] R. Dominko, D. E. Conte, D. Hanzel, M. Gaberscek, and J. Jamnik, Impact of synthesis conditions on the structure and performance of  $Li_2FeSiO_4$ , *J. Power Sources* **178**, 842 (2008).
- [10] M. E. Arroyo-deDompablo, R. Dominko, J. M. Gallardo-Amores, L. Dupont, G. Mali, H. Ehrenberg, J. Jamnik, and E. Morán, On the energetic stability and electrochemistry of  $Li_2MnSiO_4$  polymorphs, *Chem. Mater.* **20**, 5574 (2008).
- [11] M. S. Islam, R. Dominko, C. Masquelier, C. Sirisopanorn, A. R. Armstrong, and P. G. Bruce, Silicate cathodes for lithium batteries: alternatives to phosphates? *J. Mater. Chem.* **21**, 9811 (2011).
- [12] A. Nytén, S. Kamali, L. Häggström, T. Gustafsson, and J. O. Thomas, The lithium extraction/insertion mechanism in  $Li_2FeSiO_4$ , *J. Mater. Chem.* **16**, 2266 (2006).
- [13] M. Avdeev, Z. Mohamed, and C. D. Ling, Magnetic structures of  $\beta_1$ - $Li_2CoSiO_4$  and  $\gamma_0$ - $Li_2MnSiO_4$ : Crystal structure type vs. magnetic topology, *J. Solid State Chem.* **216**, 42 (2014).
- [14] V. B. Nalbandyan, E. A. Zvereva, I. L. Shukaev, E. Gordon, V. V. Politayev, M. H. Whangbo, A. A. Petrenko, R. S. Denisov, M. M. Markina, M. Tzschoppe, K.Y. Bukhteev, R. Klingeler, and A. N. Vasiliev,  $A_2MnXO_4$  Family ( $A = Li, Na, Ag; X = Si, Ge$ ): Structural and Magnetic Properties, *Inorg. Chem.* **56**, 14023 (2017).
- [15] J. Rodriguez-Carvajal, Recent advances in magnetic structure determination by neutron powder diffraction, *Phys. B (Amsterdam, Neth.)* **192**, 55 (1993).



- [16] Y. Su, K. Nemkovskiy, and S. Demirdis, DNS: Diffuse scattering neutron time-of-flight spectrometer, *J. Large-Scale Res. Facil.* **1**, A27 (2015) .
- [17] W. Schweika, XYZ-polarisation analysis of diffuse magnetic neutron scattering from single crystals, *J. Phys. Conf. Ser.* **211**, 012026 (2010).
- [18] R. L. McGreevy, Reverse monte carlo modelling, *J. Phys.: Condens. Matter* **13**, R877 (2001).
- [19] J. A. M. Paddison, J. R. Stewart, and A. L. Goodwin, SPINVERT: a program for refinement of paramagnetic diffuse scattering data, *J. Phys.: Condens. Matter* **25**, 454220 (2013).
- [20] See Supplemental Material at <http://link.aps.org/supplemental/10.1103/PhysRevB.102.214420> for details.
- [21] R. D. Shannon, Revised effective ionic radii and systematic studies of interatomic distances in halides and chalcogenides, *Acta Crystallogr., Sect. A: Cryst. Phys., Diffr., Theor. Gen. Crystallogr.* **A32**, 751 (1976) .
- [22] H. Shaked, J. Faber Jr., and R. L. Hitterman, Low-temperature magnetic structure of MnO: a high-resolution neutron-diffraction study, *Phys. Rev. B* **38**, 11901 (1988).
- [23] J. M. Perez-Mato, S. V. Gallego, E. S. Tasci, L. Elcoro, G. de la Flor, and M. I. Aroyo, Symmetry-based computational tools for magnetic crystallography, *Annu. Rev. Mater. Res.* **45**, 217 (2015).
- [24] N. V. Belov, N. N. Neronova, and T. S. Smirnova, Shubnikov groups, *Sov. Phys. Crystallogr.* **2**, 311 (1957).
- [25] S. V. Maleev, V. G. Bar'yaktar, and R. A. Suris, The scattering of slow neutrons by complex magnetic structures, *Sov. Phys. Solid State* **4**, 2533 (1963); M. Blume, Polarization effects in the magnetic elastic scattering of slow neutrons, *Phys. Rev.* **130**, 1670 (1963).
- [26] G. J. Nilsen, C. M. Thompson, G. Ehlers, C. A. Marjerrison, and J. E. Greedan, Diffuse magnetic neutron scattering in the highly frustrated double perovskite Ba<sub>2</sub>YRuO<sub>6</sub>, *Phys. Rev. B* **91**, 054415 (2015).
- [27] P. J. Saines, J. A. M. Paddison, P. M. M. Thygesen, and M. G. Tucker, Searching beyond Gd for magnetocaloric frameworks: magnetic properties and interactions of the Ln(HCO<sub>2</sub>)<sub>3</sub> series, *Mater. Horiz.* **2**, 528 (2015).
- [28] J. A. M. Paddison, H. Jacobsen, O. A. Petrenko, M. T. Fernández-Díaz, P. P. Deen, and A. L. Goodwin, Hidden order in spin-liquid Gd<sub>3</sub>Ga<sub>5</sub>O<sub>12</sub>, *Science* **350**, 179 (2015).
- [29] J. A. Paddison, Ultrafast calculation of diffuse scattering from atomistic models, *Acta Crystallogr., Sect. A: Found. Adv.* **75**, 14 (2019) .
- [30] N. Rogado, Q. Huang, J. W. Lynn, A. P. Ramirez, D. Huse, and R. J. Cava, BaNi<sub>2</sub>V<sub>2</sub>O<sub>8</sub>: A two-dimensional honeycomb antiferromagnets, *Phys. Rev. B* **65**, 144443 (2002).
- [31] I. A. Blech and B. L. Averbach, Spin correlations in MnO, *Physics* **1**, 31 (1964) .